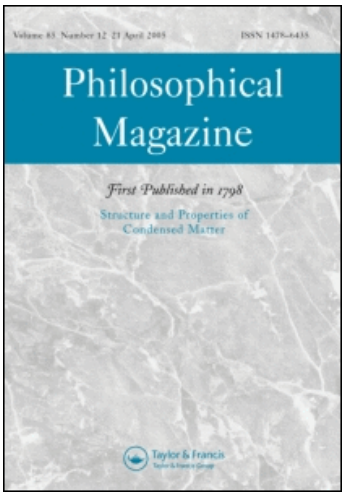

Philosophical Magazine
Publication details, including instructions for authors and subscription information:
http://www.informaworld.com/smpp/title~content=t713695589

Non-singular descriptions of dislocation cores: a hybrid ab initio continuum approach

S. Banerjee [a]; N. Ghoniem [b]; G. Lu [c]; N. Kioussis [c]
[a] Engineering Technology Department, Saint Louis University, Saint Louis, Missouri 63103-1110 [b] Mechanical and Aerospace Engineering Department, University of California, Los Angeles, California 90095-1597 [c] Department of Physics, California State University, Northridge, California 91330-8268

Online Publication Date: 01 September 2007

To cite this Article Banerjee, S., Ghoniem, N., Lu, G. and Kioussis, N.(2007)'Non-singular descriptions of dislocation cores: a hybrid ab initio continuum approach',Philosophical Magazine,87:27,4131 — 4150
To link to this Article: DOI: 10.1080/14786430701528739
URL: http://dx.doi.org/10.1080/14786430701528739

Philosophical Magazine,
Vol. 87, No. 27, 21 September 2007, 4131–4150

Taylor & Francis
Taylor & Francis Group

Non-singular descriptions of dislocation cores: a hybrid *ab initio* continuum approach

S. BANERJEE†, N. GHONIEM*‡,
G. LU§ and N. KIOUSSIS§

†Engineering Technology Department, Saint Louis University,
Saint Louis, Missouri 63103-1110
‡Mechanical and Aerospace Engineering Department,
University of California, Los Angeles, California 90095-1597
§Department of Physics, California State University,
Northridge, California 91330-8268

(*Received 19 February 2007; in final form 20 June 2007*)

The core structure of straight and curved dislocations is studied by developing a hybrid approach that links the parametric dislocation dynamics method with *ab initio* calculations. The approach is an extension of the Peierls–Nabarro (PN) model, with the following features: (1) all three components of the displacement vector for atoms within the dislocation core are included; (2) the entire generalized stacking fault energy surface (GSFS) obtained from *ab initio* calculations is utilized; and (3) the method is generalized to treat curved dislocations. We combine the parametric dislocation dynamics (DD) approach for the interaction and motion of dislocations with *ab initio* calculations of lattice restoring forces. These forces, which are extracted from the GSFS (γ-surface), are calculated from both first-principles density functional theory (DFT) and the embedded-atom method (EAM). Dislocation core structures in aluminium and silver are determined. For straight dislocations, the results from the model are shown to be in excellent agreement with experiments for both Al and Ag. In contrast to undissociated dislocation loops in Al, it is found that the core width and the separations between partials in Ag vary along the angular direction measured with respect to the Burgers vector. It is also shown that the core-cutoff radius, which is usually employed in DD calculations to avoid singularities, must be adjusted as a function of loop size to account for the correct dislocation core energy.

1. Introduction

Dislocations play a central role in understanding many key phenomena in materials science and engineering. The traditional description of elastic field and energies of dislocations is based on continuum theory of linear elasticity that suffers from the long-standing problem of singularities at the dislocation core. Singular solutions are often circumvented by introducing an artificial core-cutoff radius. This limits the applicability of the theory to describe situations where it is important to know the

*Corresponding author. Email: ghoniem@ucla.edu

Philosophical Magazine
ISSN 1478–6435 print/ISSN 1478–6443 online © 2007 Taylor & Francis
http://www.tandf.co.uk/journals
DOI: 10.1080/14786430701528739

strained state and nanoscopic details within a few atomic spacings surrounding the dislocation centre, known as the dislocation core. There has been a great deal of interest in describing accurately the dislocation core structure on an atomic scale and providing a non-singular treatment because of its important role in many phenomena of crystal plasticity. Computational methods based on direct atomistic simulations using either empirical interatomic potentials or *ab initio* calculations have been used to understand the core properties [1, 2]. Empirical potentials involve the fitting of parameters to a predetermined database and hence may not be reliable in predicting the core properties of dislocations, where severe distortions like bond breaking, bond formation and switching necessitate a quantum mechanical description of the electronic degrees of freedom. *Ab initio* total energy calculations for atoms within dislocation cores, though considerably more accurate, are computationally very demanding and not tractable at the present time. On the other hand, continuum methods based on the Peierls–Nabarro (PN) framework have been the subject of various studies due to their simple and easily accessible hybrid nature, which essentially establishes a connection between atomic and continuum length scales [3–8] and offers an attractive alternative to large-scale atomic simulations.

In the original one-dimensional PN model of a straight dislocation, it is assumed that the dislocation with Burgers vector b, conveniently represented as a continuous distribution of infinitesimal dislocations, is confined on a single slip plane (glide plane) separating two semi-infinite linear elastic continua. The PN equation for the relative slip displacement, $u(x)$, of the upper half of the crystal with respect to the lower half at point x (which is the coordinate of the atomic row parallel to the dislocation line) is obtained by requiring balance of the shearing stresses, due to such infinitesimal dislocations at x' and the nonlinear atomic restoring stress $\sigma_p[u(x)]$, acting across the glide plane [9]. The model does have the great merit of providing an analytical nonlinear elastic solution of a dislocation core, which eliminates the singularity at the origin [10]. The original PN model is based on an assumed sinusoidal form for the lattice resistance (known as Frenkel relation [11]), which gives

$$u(x) = \frac{b}{2} + \frac{b}{\pi}\tan^{-1}\frac{x}{\xi} \tag{1}$$

where $\xi = Kb/2\tau_{\max}$ is the half width of the dislocation core and $\tau_{\max}$ is the maximum restoring stress.

The model, however, suffers from a serious shortcoming, especially, in modelling solids with a narrow core (as is typically the case in covalently bonded solids), due to its unrealistic use of Hooke's law in the restoring stress calculations at the highly nonlinear core region [10]. The original PN model has played a dominant role in recent years after the introduction of the concept of the generalized stacking fault (GSF) (or gamma-γ) surface [12]. The γ-surface can be interpreted as the two-dimensional energy profile when the two crystal halves above and below the glide plane are shifted rigidly against each other by a constant disregistry vector, $\boldsymbol{u}$, and the atoms are allowed to relax normal to the glide plane. For a disregistry vector $\boldsymbol{u}$, there is an interfacial restoring stress

$$\mathbf{F_r}(\mathbf{u}) = -\nabla(\gamma(\mathbf{u})) \tag{2}$$

which has the same formal interpretation as the restoring stress in the PN model. The GSF energies can be calculated using empirical interatomic potentials such as the embedded-atom method (EAM) and recently, using the electron density functional theory (DFT) *ab initio* calculations.

The extension of the original PN model in one dimension embedding specific information from the GSF energy surface has been carried out by a number of investigators [6, 7, 13, 14]. In two dimensions, the force balance would require two complicated coupled integro-differential equations for the slip displacements, which can be solved numerically by tedious iterative procedures as suggested by [15]. Recently, two methodologies have been proposed in two dimensions to study dislocation dissociation in metals or alloys. Both approaches require that the total energy composed of elastic and atomic misfit contributions must be minimized to obtain the equilibrium structure of the core. In [4], a semidiscrete variational method (SVM) is presented, where the dislocation energy functional is expressed in terms of the unknown edge, normal, and screw components of the general interplanar displacement density at nodal points by an explicit discretization of energy terms. On the other hand, a concept of Peierls type dislocations was introduced by Schoeck [16], where the displacement vector is represented by a set of trial functions that contain a number of adjustable geometrical parameters, whose value is determined by minimizing the total energy. While these models provide great physical insights into the analysis of the dislocation core, they are restricted to straight dislocations so far.

Computational methods based on continuum models to treat dislocation loops of arbitrary shape are rather sparse. A variational boundary integral method has been used for the analysis of three-dimensional cracks with arbitrary geometry by representing them as continuous distributions of dislocation loops [17]. The PN model enters into this approach by refining the sinusoidal restoring stress law to study the homogeneous nucleation of dislocations from crack tips [18], and the slip distribution is obtained by minimizing the total energy. As a result, the model has not been used for crystals where dislocations are highly dissociative in nature. It should also be noted that there are several other models that are based on the non-singular continuum theory of dislocations (e.g. [19–21]), but they do not take into account any direct information from atomistic calculations. Such models use a Burgers vector spreading parameter along the dislocation line itself.

In this paper, we present a computationally tractable approach based on the direct interaction and motion of dislocations, known as dislocation dynamics. Developed over the past two decades, DD is a direct approach that attempts to simulate the aggregate behaviour of large dislocation ensembles and holds considerable promise for uncovering the microscopic origins of crystal strength [22–26]. We will utilize this powerful tool to obtain the core structure of the original dislocation which is represented by arrays of Volterra dislocations of *infinitesimally* small Burgers vector. The core structure is determined by seeking an equilibrium configuration of these *fractional* dislocations via force balance. In general, for a dislocation of 3-D geometric shape, these forces are of four types: (1) applied external forces; (2) long-range interaction forces with other dislocations; (3) self-forces as a result of curvatures of dislocations; and (4) lattice restoring forces that control separation or sliding across the glide plane, and are determined from

the γ surface. The major advantage of the proposed model is that the interaction force terms for Volterra dislocations are readily available for a number of classic problems, e.g. dislocation transmission across interfaces, dislocation interaction with a precipitate, dislocation cross slip, etc. [27–31]. In order to explore the reliability and versatility of the approach, we study the core structure of two distinctive fcc metals, Al and Ag. The gamma surfaces are calculated using both DFT and EAM. The general trend for the presence or absence of dissociation into partials will be discussed both for the straight and curved dislocations.

2. Atomistic-dislocation dynamics model

2.1 *Straight dislocations*

We choose an appropriate right handed coordinate system as shown in figure 1. The dislocation line vector is along the z-axis and the Burgers vector, perpendicular to the y-axis, makes an angle θ with the z-axis. The Burgers vector is along the x-axis ($\theta = 90^{\circ}$) for an edge dislocation and along the z-axis ($\theta = 0^{\circ}$) for a screw dislocation. The Burgers vector of a mixed dislocation has both an edge component, $b_e = b \sin\theta$, and a screw component, $b_s = b \cos\theta$. In general, the atomic displacement vector has components in all three directions rather than only along the direction of the Burgers vector. Atomic displacements along the Burgers vector may have to surmount a higher inter-planar energy barrier in the GSF surface than along alternate directions. In other words, the GSF energy is reduced when the dislocation acquires additional displacement components in other directions. For the purpose of this paper, we assume that the core is confined within the glide plane xz so that the out of plane displacement component, u_y, is ignored. In fact, this assumption is not an over-simplification in the context of the current problem. The previous calculations using

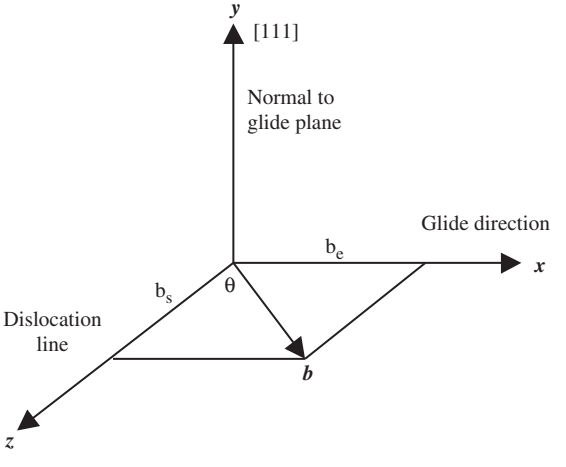

Figure 1. The Cartesian coordinate system used in the simulation showing the relevant directions for dislocations in Al and Ag.

a semidiscrete variational model [4] show that this component of displacement is very small and unimportant for planar dislocations. The other two components of the slip displacements, u_x and u_z, are connected to the positions of fractional dislocations of edge and screw type with fractional Burgers vectors, which are used to represent the core of the original dislocation using a suitable basis function. The structure of the dislocation core is obtained by seeking the equilibrium configuration of these fractional Volterra dislocations. Physically this corresponds to balancing the elastic forces and the lattice restoring forces across the glide plane as envisioned in the original PN model.

Consider a mixed dislocation of Burgers vector $\mathbf{b} = b^{\mathrm{e}}\hat{\mathbf{e}} + b^{\mathrm{s}}\hat{\mathbf{s}}$, where $\hat{\mathbf{e}}$ and $\hat{\mathbf{s}}$ are unit vectors along the edge and screw directions, respectively. If the Burgers vector makes an angle θ with respect to the dislocation line (y-axis), then $b^e = b\sin\theta$ and $b_s = b\cos\theta$. The displacement field of the original dislocation can be represented as a superposition of the displacement fields from the fractional dislocations on the same glide plane:

$$u^{\mathrm{e}} = \sum_{i=1}^{N} b_i^{\mathrm{e}} \tan^{-1}\left(\frac{x - x_i}{\xi^e}\right) + \frac{b^{\mathrm{e}}}{2} \tag{3}$$

$$u^{\mathrm{s}} = \sum_{j=1}^{N} b_j^{\mathrm{s}} \tan^{-1}\left(\frac{x - x_j}{\xi^s}\right) + \frac{b^{\mathrm{s}}}{2} \tag{4}$$

$$u_z = 0. \tag{5}$$

Here $b_i^{\mathrm{e}} = b^{\mathrm{e}}/N$, $b_j^{\mathrm{s}} = b^{\mathrm{s}}/N$ are the Burgers vectors of the fractional dislocations with a total of N dislocations for each type; x_i, x_j are their positions on the glide plane, respectively, and ξ^e, ξ^s are the usual core-cutoff (core width) that are set to half of the fractional Burgers vector. The elastic force on the ith dislocation of edge type can be written as

$$f_i^E = \sum_{k \neq i}^{N} b_i^{\mathrm{e}} \frac{\mu}{2\pi(1-\nu)} \frac{1}{x_i - x_k} \tag{6}$$

On the other hand, the lattice restoring force is given by

$$f_i^L = b_i^{\mathrm{e}} \frac{\partial \gamma}{\partial u_e}|_{x=x_i} \tag{7}$$

Similarly, on the jth dislocation of screw type the elastic force and the lattice restoring force are given by,

$$f_j^E = \sum_{k \neq j}^{N} b_j^{\mathrm{s}} \frac{\mu}{2\pi} \frac{1}{x_j - x_k} \tag{8}$$

$$f_j^L = b_j^s \frac{\partial \gamma}{\partial u_s}|_{x=x_j} \tag{9}$$

The position of the fractional dislocations of edge and screw type are updated within the setup of dislocation dynamics through the usual relationships

$$f_i^E + f_i^L = Bv_i \tag{10}$$

$$f_j^E + f_j^L = Bv_j \tag{11}$$

where v_i and v_j are the velocities of the edge and screw type dislocations, respectively, and B is the mobility of the dislocations, which is artificially introduced to update the position of dislocations at a time step. Simulations are carried out until the velocity of each fractional dislocation vanishes, i.e. the dislocations glide to their equilibrium configuration, which ensures that the force equilibrium is achieved. Equations (10, 11) also suggest that there is always a unique equilibrium configuration for any given initial configuration. However, the initial configuration cannot be chosen arbitrarily in order to maintain a low computational time for the dislocations to reach the equilibrium configuration. As an initial configuration, we have set a uniform spacing of the fractional dislocations through all simulations. Once the final positions of the fractional dislocations are known, the components of the dislocation density can be calculated using (3) as $\rho_e = du^e/dx$, $\rho_s = du^s/dx$, to interrogate the splitting of the core into partials. In order to examine the displacement or dissociation path (so called minimized energy path) the components of the displacement vector parallel (u^b) and perpendicular (u^p) to the Burgers vector can also be calculated using the usual transformation, i.e. $u_b = u^e \sin\theta + u^s \cos\theta$ and $u^p = u^e \cos\theta - u^s \sin\theta$.

In order to capture the partial splitting for a pure edge dislocation, a null set, composed of positive and negative fractional screw dislocations is introduced into the same glide plane. The number of the positive fractional screw dislocations is identical to that of the negative fractional screw dislocations so that the net Burgers vector of the system remains the same. Since there is no cross elastic interaction between the edge and screw dislocations, they can move independently, as far as the elastic energy is concerned. Representing different displacement directions, these edge and screw dislocations could experience very different lattice restoring forces, depending on the detailed structure of the GSF energy surface. To minimize the total energy (elastic plus misfit energy) of the system, some of these oppositely signed screw dislocations may annihilate while the edge dislocations may cluster. The resultant displacement field due to the original edge dislocation is thus determined by the superposition of the displacement fields from all fractional dislocations (edge and screw) present in the simulation. The original edge dislocation dissociates into two partials if a certain number of screw dislocations survives; the location of the partials corresponds to where the segregation of the edge dislocations occurs. The procedure remains the same for the simulation of a perfect screw dislocation, but with oppositely signed edge dislocations introduced instead. It should be noted that the final solution does not depend on the basis function ($\tan^{-1}$ type) used in equations (3). However, the basis function should lead to a smooth curve with sufficient number of dislocations used in the arrays and thus results in a non-singular elasticity solution for the core. It should also be pointed out that if the two fractional dislocations want to approach at distances smaller than the core-cutoff dimension,

the elasticity equations are still used with the core-cutoff width ($b/2N$) being the distance between them. It is envisioned that the magnitude of the elastic field exerted by a fractional dislocation is very small since its burgers vector is also infinitesimally small, and the overall solution for the core converges as we take the limit of an infinite number of infinitesimal dislocations. The fact that the core has 'small singularities' is just a computational convenience. It will be shown that the results from the present approach agrees well with those obtained from the semidiscrete variational model proposed earlier [4].

2.2 *Dislocations loops*

The extension of the model to 3D is not trivial, and simplified assumptions, especially in determining the displacement path, will be made a priori. In fact, such assumptions come out naturally from the results of straight dislocations with dissociated or undissociated cores. We briefly describe here the 3D PDD method and show schematics illustrating our approximation.

In the 3D PDD method each dislocation segment is represented by a parametric space curve of specified shape functions and associated degrees of freedom. It has been shown that the evolution equations for the position (**P**), tangent (**T**), and normal (**N**) vectors at segment nodes are sufficient to describe general 3D dislocation motion [26]. The resulting sets of ordinary differential equations, describing the motion of an ensemble of dislocation loops as an evolutionary dynamical system, can be written in a global matrix form as

$$\mathbf{F}(\mathbf{Q}) = \mathbf{B}\frac{d\mathbf{Q}}{dt} \tag{12}$$

Here **Q** represents a set of generalized coordinates, **B** is the resistivity matrix and the elements of **F(Q)** are the force acting on any node, taking into account contributions resulting from the loop itself (i.e. the self-force), from other dislocations (i.e. the interaction force), the externally applied force, and the lattice restoring force. The expressions for the elastic fields can be found in [25] as fast numerical sums over the loop segments (N_s) and Gaussian quadrature points ($Q_{\max}$) associated with the weighting factors (w_α). We summarize the results below as necessary. The stress field is given by

$$\sigma_{ij} = \frac{\mu}{4\pi}\sum_{\beta=1}^{N_s}\sum_{\alpha=1}^{Q_{\max}} b_n w_\alpha \left[\frac{1}{2}R_{,mpp}\left(\in_{jmn}\hat{x}_{i,u} + \in_{imn}\hat{x}_{j,u}\right) + \frac{1}{1-\nu}\in_{kmn}\left(R_{,ijm} - \delta_{ij}R_{,ppm}\right)\hat{x}_{k,u}\right] \tag{13}$$

and the elastic interaction energy is

$$E_I = -\frac{\mu b_i^{(1)} b_j^{(2)}}{8\pi}\sum_{\beta^{(1)}=1}^{N_s^{(1)}}\sum_{\beta^{(2)}=1}^{N_s^{(2)}}\sum_{\alpha^{(1)}=1}^{Q_{\max}^{(1)}}\sum_{\alpha^{(2)}=1}^{Q_{\max}^{(2)}} w_{\alpha^{(1)}} w_{\alpha^{(2)}} \times \left[R_{,kk}\left(\hat{x}_{j,u}^{(2)}\hat{x}_{i,u}^{(1)} + \frac{2\nu}{1-\nu}\hat{x}_{i,u}^{(2)}\hat{x}_{j,u}^{(1)}\right) + \frac{2}{1-\nu}\left(R_{,ij} - \delta_{ij}R_{,ll}\right)\hat{x}_{k,u}^{(2)}\hat{x}_{k,u}^{(1)}\right] \tag{14}$$

Here $\hat{\mathbf{x}}$ is the position vector for any point on the parametric segment. If the position of any other point in the medium is defined as $\mathbf{x}$, then the vector connecting the source point, $\hat{\mathbf{x}}$, to the field point, $\mathbf{x}$, can be described as $\mathbf{R} = \hat{\mathbf{x}} - \mathbf{x}$, so that $R = \|\mathbf{R}\|$. ε is the usual permutation tensor and δ is the Kronecker delta.

The lattice restoring force is embedded into the model through (2) after some simplifications based on the straight dislocation results. It will be shown that the displacement path tends to be along the Burgers vector direction in case of an undissociated core, whereas, in case of a dissociated core it tends to follow the direction of the patrials Burger vector. Since a dislocation loop can be viewed as the composition of straight dislocation segments, its basic behaviour is presumed to follow the same rule. Therefore, for an undissociated dislocation loop the restoring stress profile corresponding to the projection of the DFT energy surface along the Burgers vector direction is adequate for the present calculations. Similarly, for a dissociated dislocation loop, the projection of the DFT energy surface along the partial directions is sufficient. This leads to the constrained path approximation [18], which has been used elsewhere [17]. Therefore, the slip displacement for each loop representing the core can be approximated. For example, if N is the total number of dislocations used to represent the core of an undissociated loop, each having a Burgers vector b/N, then the slip displacement, $u_x = u$, along the Burgers vector direction (assumed to be x-direction), can be set for each one using the step function approximation. Note that the other components of the displacements are set to zero and that the component u_x is independent of the angular coordinate, θ, in a polar coordinate representation. Then the lattice restoring forces for each fractional dislocation loop is fully determined. Similarly, the core of a dissociated loop can be represented by means of two groups of loop arrays, such that each loop in one group has a Burgers vector of b_1/N_1 and in the other group has a Burgers vector of b_2/N_2, where b_1 and b_2 are the dissociated Burgers vectors and N_1 and N_2 are the number of dislocations representing each group. In this case, the slip displacements, u_x and u_y (say) will have both components, but they are again independent of θ. Schematics of such representations are shown in figure 2

3. Results and discussions

In this section, we present results of calculations of the dislocation core structure for ideal bulk aluminium (Al) and silver (Ag) crystals. The dislocations are assumed to be confined in the (111) glide plane with $b = \frac{1}{2}[101]$ direction. The materials properties and Burgers vectors for the two crystals are tabulated in table 1.

3.1 *Straight dislocations*

In order to prove the validity and versatility of the model, we first carry out a comparative study of the planar dissociation in Al using DFT and EAM gamma surfaces and verify the results with the SVM and experimental observations

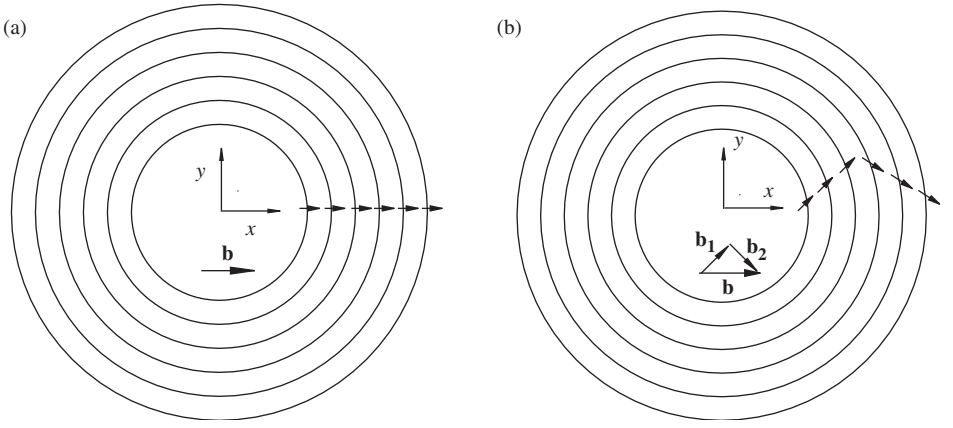

Figure 2. Schematic representation of the loop arrays for (a) undissociated core, (b) dissociated core. The orientation of the predefined distributed burgers vectors for each loop is shown for both cases.

Table 1. Materials properties for the FCC lattices used in the simulations.

FCC	μ (GPA)	ν	b (A^{o})
Al	28.8	0.344	2.8053
Ag	33.8	0.354	2.8323

published elsewhere. The results are further extended to Ag using DFT energy surface to contrast the dislocation structure.

3.1.1 Dislocation structure in Al. The GSF energy surface for displacements along (111) plane in Al is calculated within the framework of DFT in the local-density approximation to the exchange-correlation functional using the expression proposed by Perdew and Zunger [32]. For the EAM calculations of the GSF energy surface, the Ercolessi–Adams potential is used. The fitted GSF energy surface from the DFT and EAM, is shown in figure 3.

The three high peaks of the GSF surfaces correspond to the run-on stacking fault configuration $ABC|CABC$, in which two C layers are neighbouring each other. The first energy maximum encountered along the $[12\bar{1}]$ direction is the unstable stacking fault energy, which represents the lowest energy barrier for dislocation nucleation and the first energy minimum at $a_0/\sqrt{6}$ (a_0 is the lattice constant calculated to be 3.94Å) corresponds to the intrinsic stacking fault configuration, where a full dislocation dissociates into a pair of Shockley partials. The ISF energy obtained from the DFT and EAM gamma surface are 0.165 and 0.120 J/m^2, respectively. In both the DFT and EAM calculations, the unstable stacking-fault energy along [101] is found to be larger than that along $[12\bar{1}]$.

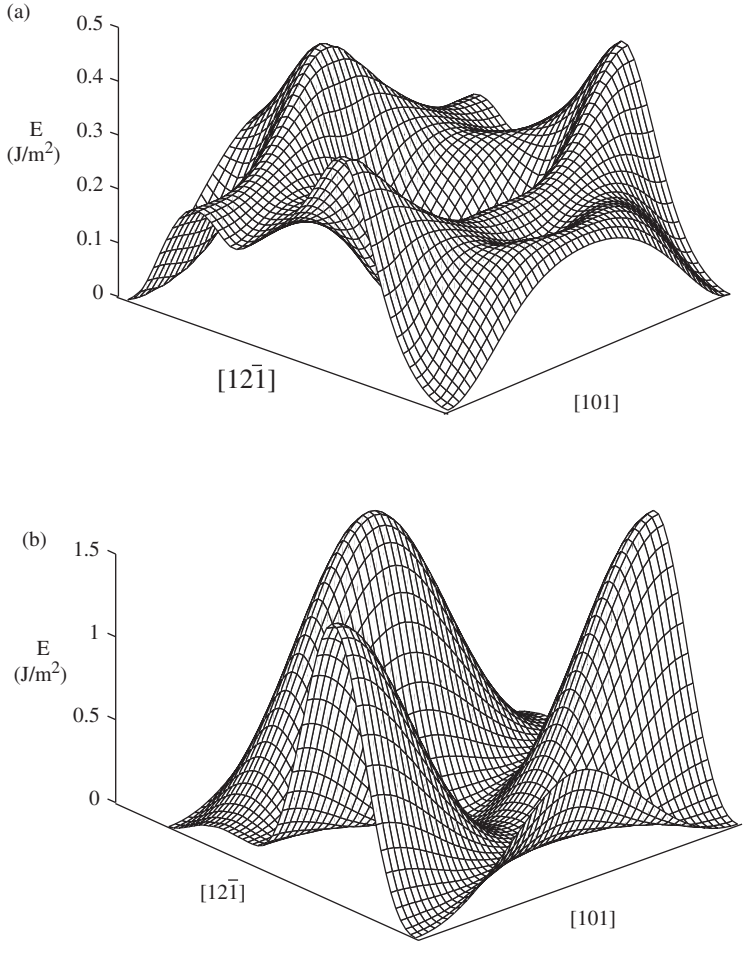

Figure 3. The GSF energy surface for displacements on a (111) plane in Al in J/m^2 (the corners of the plane and its centre correspond to identical equilibrium configurations, i.e. the ideal Al lattice) (a) from DFT pseudopotential plane-wave calculations; (b) from EAM calculations.

In figure 4, we compare the dislocation density for 90° (edge) and 60° dislocations utilizing the DFT γ surface from the two approaches, namely, the atomistic-DD model and semidiscrete variational model [4]. The corresponding dissociation paths (so called minimized energy path) along and perpendicular to the Burgers vector are also shown in figure 5. Good agreement between the results from the two approaches are found. Both models using DFT predict no splitting for the complete dislocation into partials, consistent with experiment [34]. Minor displacement components perpendicular to the Burgers vector (u^p), however, suggests that a full dislocation may split into two highly overlapped partials (figure 5).

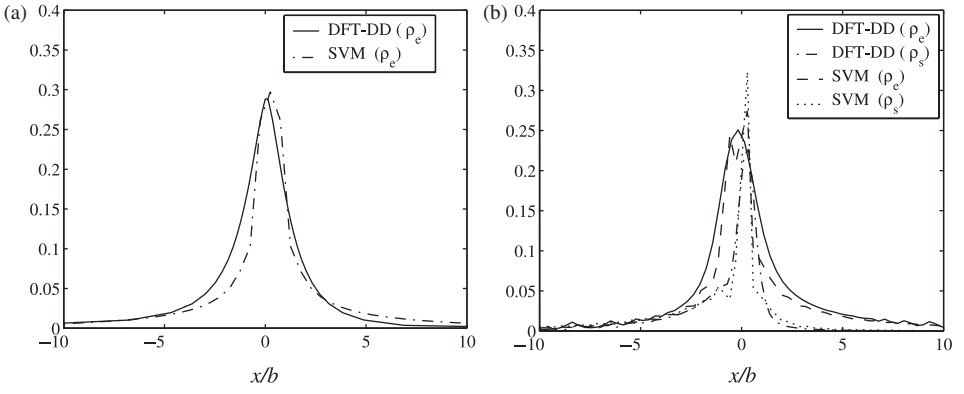

Figure 4. Dislocation density for (a) an edge dislocation and (b) a 60° dislocation obtained from the two models. A DFT γ surface is used in both cases.

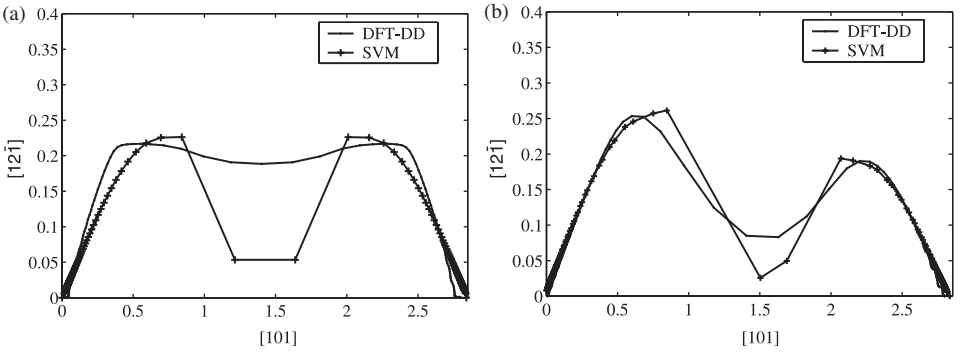

Figure 5. Displacement paths in units of (Å) along and perpendicular to the Burgers vector direction for (a) an edge dislocation and (b) a 60° dislocation obtained from the two models. A DFT γ surface is used in both cases.

Table 2. Comparison of core width in units of b from the semidiscrete variational method [4] and the present model for straight dislocations.

Method	0°	30°	60°	90°
Semidiscrete	1.5	1.78	2.14	2.5
Present	1.52	1.84	2.18	2.53

In order to check the convergence of the present model, the number of dislocations in the array is gradually increased. It is found that a fairly accurate solution can be obtained using 25 or even fewer dislocations, when compared with the semidiscrete variational method. The two methods are found to agree within an average disregistry error of 2.5% for 10, 1.2% for 15, and 0.05% for 25 dislocations. The dislocation core width, defined as the atomic distance over which u changes from $b/4$ to $3b/4$, are compared in table 2 from the two models for 25 dislocations. The core width may also be calculated assuming a sinusoidal

form of the restoring stress [10]. As indicated by Lu *et al.* [4], while the first definition takes into account the entire gamma surface, the second definition involves only the maximum restoring stress, which can be set equal to the first maximum of the restoring stress, encountered along the $[12\bar{1}]$ direction. However, the excellent agreement between the values of the core width from the two definitions suggests that the details of the GSF surface are not important in the evaluation of the core width.

The results using the EAM gamma surface are displayed in figures 6 and 7. It is interesting to examine the character of the resultant partials here. The complete edge dislocation dissociates into two symmetric 60° partials, whereas the 60° dislocation dissociates into a 30° and a 90° partial. The double-peak structure in the SVM stems from non-equivalent nodal spacings between neighbouring atomic planes. The fact that the density of the screw component vanishes at the point where the edge component reaches its maximum is indicative of the pure edge character

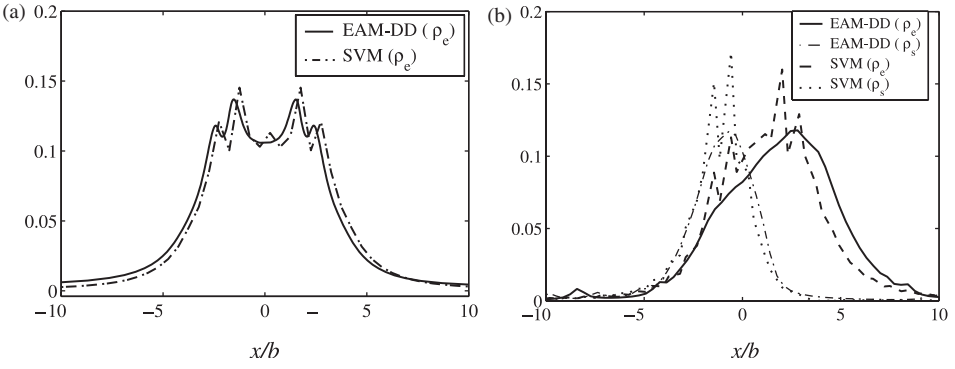

Figure 6. Dislocation density for (a) an edge dislocation and (b) a 60° dislocation obtained from the two models. An EAM γ surface is used in both cases.

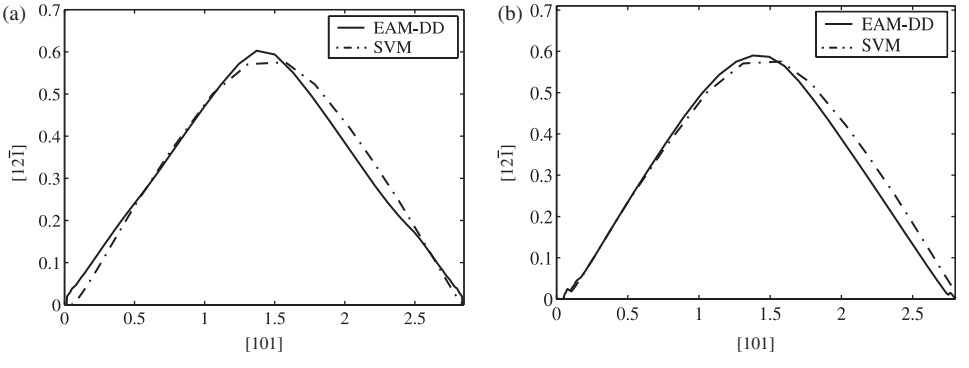

Figure 7. Displacement paths in units of (Å) along and perpendicular to the Burgers vector direction for (a) an edge dislocation and (b) a 60° dislocation obtained from the two models. An EAM γ-surface is used in both cases.

of the 90° partial. In both cases, major displacement components perpendicular to the Burgers vector are suggestive of full dissociation of the Burgers vector.

In contrast to DFT results and experiment, the EAM calculations predict that the full edge and 60° dislocations dissociate into partials. Our result for the dissociation of the full 60° dislocation into partials agrees with direct atomistic simulations using the same Ercolessi–Adams EAM potential. Although this agreement indicates the success of the models in predicting the finer core structure, the result itself is not consistent with the experiment due to the smaller ISF energy obtained from EAM calculations. It is also interesting to compare our results to recent atomistic simulations of Mills *et al*. [33]. Employing the same Ercolessi–Adams EAM potential, Mills *et al*. [33] determined the core spreading of the 60° dislocation, which in turn gives an ISF energy of 0.120 J/m^2, in excellent agreement with our EAM value. Furthermore, these authors conclude that empirical EAM potentials are not capable of accurately modelling the dissociation of the 60° dislocation. The successful application of the model to aluminium further proves its reliability for other materials. We choose Ag for another test.

3.1.2 Dislocation structure in Ag. It has already been justified that the results using the DFT γ-surface predict accurate core structures. Therefore, for Ag we present the results using the DFT γ-surface, which is shown in figure 8. The most striking difference between the DFT γ surfaces of Ag and Al is the large difference in the intrinsic stacking fault energy, which is only 0.014 J/m^2 for Ag. This dramatic difference in the γ-surface gives rise to very different dislocation core structures as will be seen next. The dislocation density for screw and 30° dislocations are presented in figure 9. The corresponding dissociation paths are shown in figure 10. Noticeably, a full screw dislocation tends to dissociate into two 60° partials. The partial separation distance we obtained from the model calculation is in an excellent agreement with the TEM measurement [35] and SVM calculations reported earlier [30] for that in Ag, which is about 20Å. Obviously, the lack of a clear dissociation in

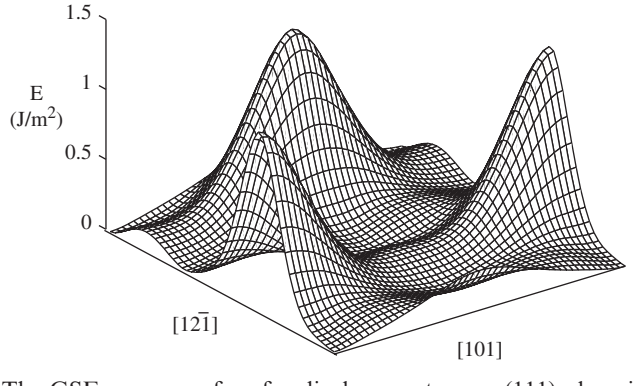

Figure 8. The GSF energy surface for displacements on a (111) plane in Ag in J/m^2.

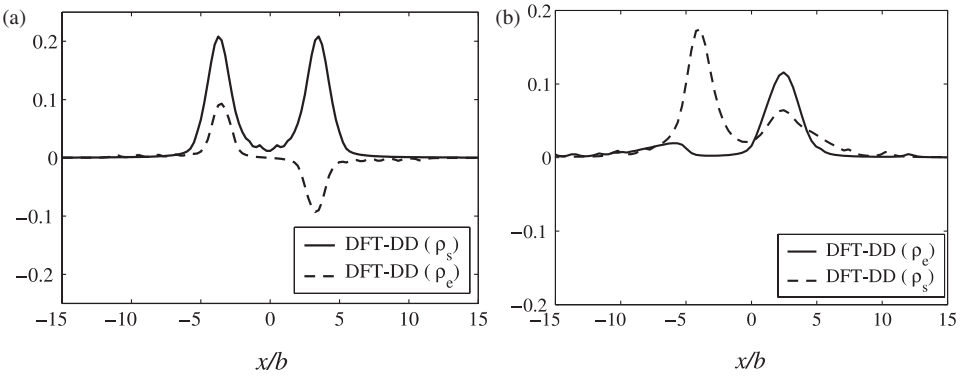

Figure 9. Dislocation density for (a) an edge dislocation and (b) a 30° dislocation obtained from the two models. A DFT γ-surface is used in both cases.

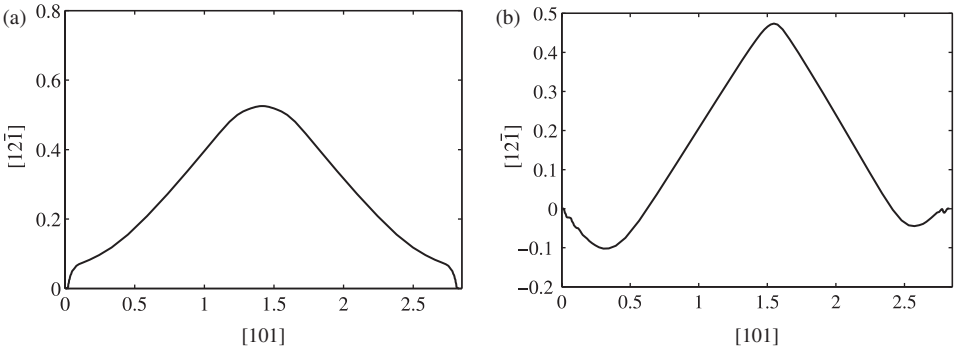

Figure 10. Displacement paths in units of (Å) along and perpendicular to the Burgers vector direction for (a) an edge dislocation and (b) a 30° dislocation obtained from the two models. A DFT γ surface is used in both cases.

Al results from the fact that the intrinsic stacking fault energy in Al is much higher than that in Ag.

3.2 *Dislocation loops*

3.2.1 Undissociated dislocation structure in Al. Unlike a straight dislocation, an externally applied stress field is required to stabilize the core structure of a dislocation loop as a result of the self-force tending to collapse the loop. A uniform shear stress is applied along the Burgers vector direction (chosen as the x-direction). For an applied shear stress level, the equilibrium configuration of a nucleated dislocation loop with Burgers vector, b, is obtained. The core structure of the original dislocation loop at a given applied shear stress level can now be determined from the equilibrium configuration of loop arrays of infinitesimally small Burgers vector as discussed earlier. Note that the schematic representation of figure 2a is used to

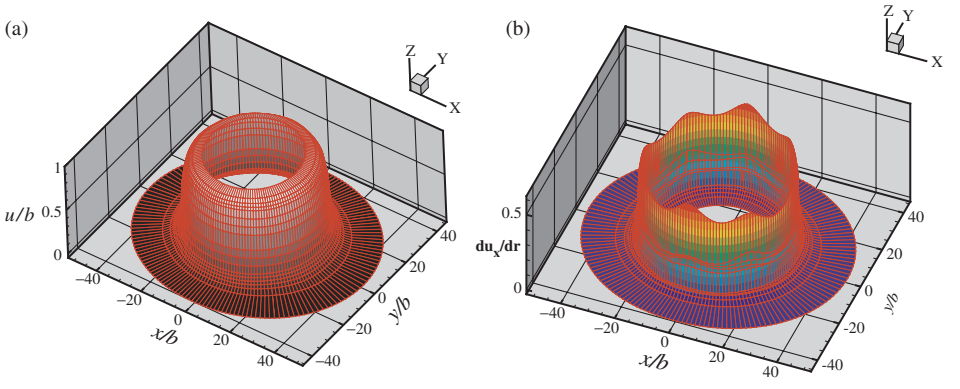

Figure 11. (a) The 3D representation of the core structure as a function of the disregistry vector, u, obtained from the equilibrium configuration of the loop arrays under an applied shear stress level of 0.018μ (540 MPa). (b) Dislocation density obtained from the equilibrium configuration.

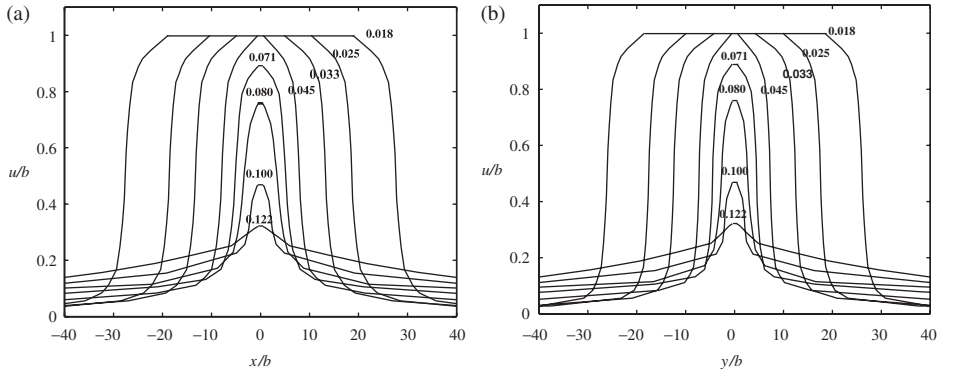

Figure 12. The (a) edge component (b) screw component of the core structure under various applied shear stress levels in units of μ.

determine the magnitude and orientation of the Burgers vector of the fractional dislocation loops. The slip displacement, u, constructed from the equilibrium configuration of the loop arrays and the corresponding dislocation density are shown in figure 11 for an applied shear stress of 0.018 μ (540 MPa).

It is seen that the density is maximum along the screw direction (y-direction) rather than the edge direction. This illustrates that the screw component of the core is tighter than the edge component. Since the loop is composed of several segments (a total of eight segments in the case) connected to each other, a few high density peaks are observed due to the confinement of these segments. Smooth variations in the density can be obtained with increasing number of segments, but can be computationally expensive. Figures 12a and b illustrate the structure of the core along the x-axis (edge component) and y-axis (screw component), respectively, at various levels of applied shear stresses. The numbers associated with each curve

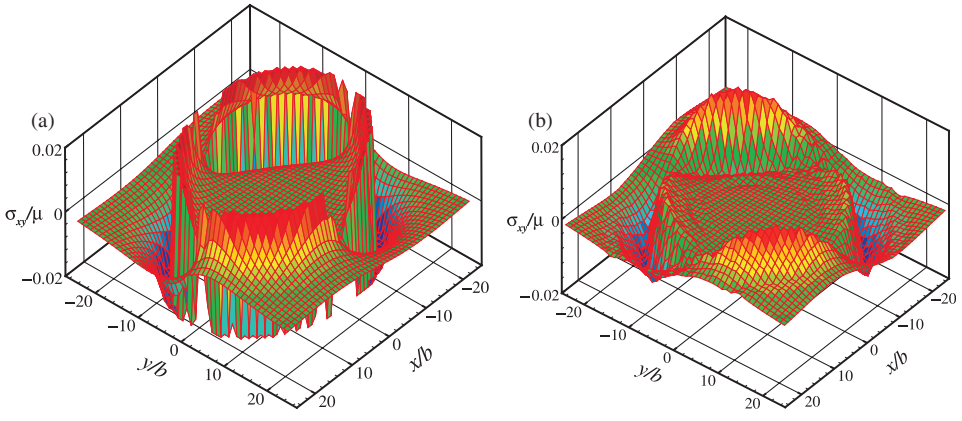

Figure 13. Comparison of the stress component, $\sigma_{xy}(x, y, 0)$, under an applied shear stress of 0.025 μ: (a) the elasticity solution; (b) the PN model.

correspond to the stress levels in units of the shear modulus μ. The core widths of the edge and screw components are found to be $2.0b$ and $1.4b$, respectively, with a negligible variation up to a certain stress value (e.g. 0.045 μ). Above the critical stress value, the loop size is very small and the core width is undefined due to the annihilation of the representative loop arrays at the centre of the loop. However, homogenized spreading of the core is clearly observed above a critical stress value. The results of our simulations are consistent with earlier theoretical work on the homogeneous nucleation of small dislocation loops under stress in perfect crystals [36].

As indicated earlier, one of the main features of the PN model is the absence of any singularities in the elastic fields. figure 13 shows the distribution of the stress component, $\sigma_{xy}(x, y, 0)$, obtained from the elasticity solution (original dislocation loop) and the PN model (dislocation arrays with fractional Burgers vector). The elimination of the singularity is clearly depicted in figure 13b.

3.2.2 Dislocation energy and core-cutoff radius. It is of interest to compare the self-energy of the original dislocation loop and its representative core structure. Within the classical elasticity framework, the self-energy of a single dislocation loop can be calculated as half the interaction energy (equation 14) between two identical coaxial dislocation loops of the same Burgers vector separated by a distance r_0. The solution contains a logarithmic divergence of the self-energy, as r_0 tends to zero. In a fairly rough evaluation, r_0 is taken as $b/2$ [37] to 'subsume' the core energy into the elasticity solution without doing any atomistic calculations. Within the PN framework, the self-energy is calculated from the direct interaction of the dislocation loop arrays using equation (14), which predicts finite core energies. In figure 14, the normalized self-energy is plotted against the major axis of the original dislocation loop from the two models.

The elasticity solution deviates greatly, especially, for large loop sizes. However, the core contribution can be incorporated into the elasticity solution by adjusting the value of r_0 as presented in figure 15. This is done by setting the elasticity solution

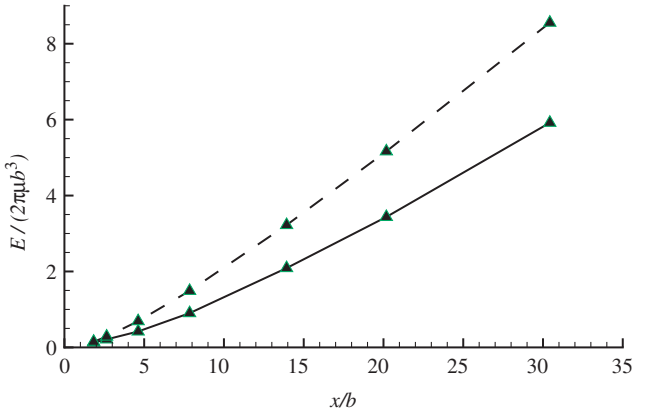

Figure 14. Variation of the self-energy of the original dislocation loop with $r_0 = b/2$ (elasticity solution, dashed line) and its representative core structure (PN model, solid line) versus the loop major axis.

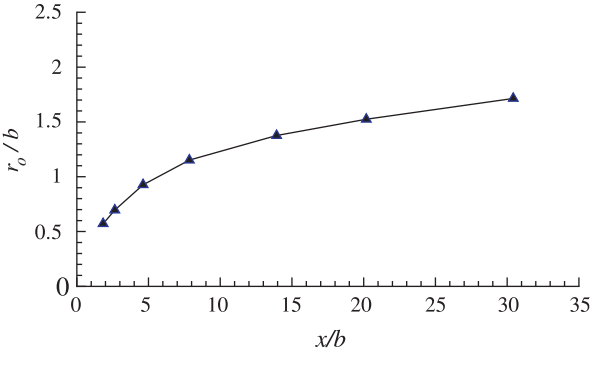

Figure 15. Variation of the core-cutoff parameter r_0 in the elasticity solution with loop size to account for the atomistic part of the core energy.

equal to the PN solution and 'calibrating' r_o in the elasticity solution to obtain the same energy as that of the PN model. The major finding is that the core-cutoff distance in the elasticity solution varies with the loop size, and tends to saturate for large loop sizes that suitably resemble the case when the line tension is small. As a consequence, large-scale dislocation dynamics simulation can account for core energy effects by adjustment of the cut-off distance with loop size. For example, large loops in DD simulations would have a cut-off core size of about $2b$, while very small loops would have a core of only $b/2$. This establishes a physical basis to adjust the core-cutoff parameter in mesoscopic DD simulations to give consistent energy with minimum computational effort.

3.2.3 Dissociated dislocation structure in Ag. The dissociative nature of a dislocation loop in Ag is studied with the goal of understanding the nature of partial separation. A uniform shear stress is applied along the [101] direction

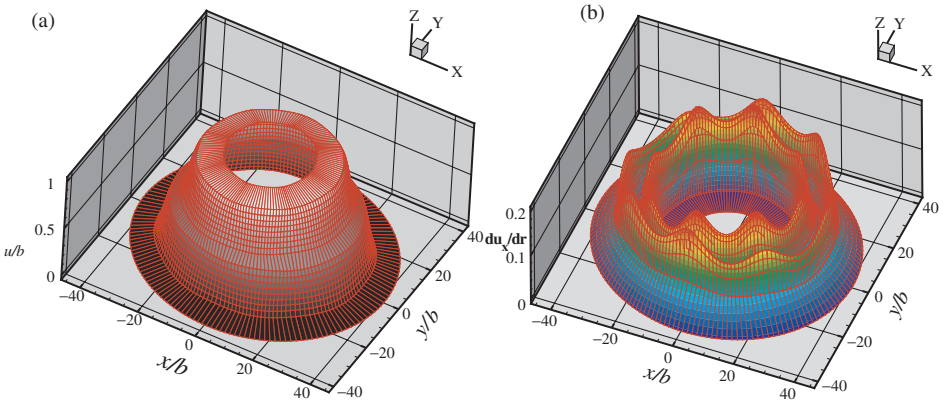

Figure 16. (a) 3D representation of the core structure as a function of the slip displacement, u_x, obtained from the equilibrium configuration of the loop arrays under an applied shear stress level of 525 MPa. (b) Dislocation density obtained from the equilibrium configuration.

(chosen as the x-direction) and the equilibrium configuration of the loop arrays is obtained. The magnitude of the applied stress is 525 MPa and the equilibrium configuration of the fractional dislocation loops is obtained. Note that for Al the schematic representation of figure 2a is used to determine the magnitude and orientation of the Burgers vector of the fractional dislocation loops, whereas, for Ag, the schematic representation of figure 2b is used. From the equilibrium configuration, the slip displacement, u, can be constructed in a trivial manner as discussed earlier (see figure 16a). The density of the slip displacement component u_x along the radial direction can now be plotted as shown in figure 16b. A clear separation between the two groups of partials is obtained in the case of Ag. Noticeably, the structure of the edge component of the core, which is along the partial Burgers vector direction for each group, is wider than the screw component.

In order to explore the nature of the dissociation in Ag, we plot the core separation in polar coordinates in figure 17. The core separation is obtained as the peak to peak separation of the density plot. It is observed that the core separation tends to be broader along an axis which is tilted relative to the x-axis. The results of our simulations for the dissociation can be easily viewed in terms of the approximate elasticity solution, where only two partials are allowed to separate by the stacking fault in between, which has been used to resolve an important class of problems [38]. The method adopted in this paper, however, provides a physical basis to resolve the fine structure of the core within the limits of the PN model and removes any artificial singularity introduced in the elasticity based solutions.

4. Concluding remarks

A new model is presented to study the core structure of 3D dislocations by integrating the local atomistic nature derived from atomistic methods into the computational framework of PDD simulations. For straight dislocations, it is

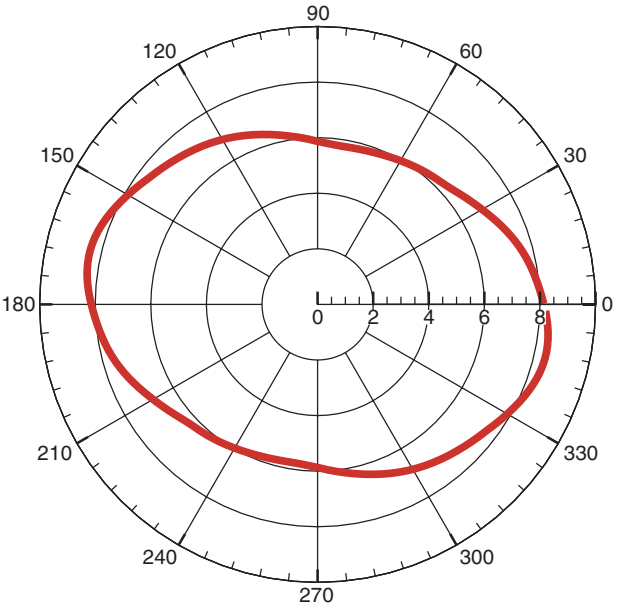

Figure 17. The core separation distance in units of b, represented in polar coordinates for Ag obtained from figure 16b.

demonstrated that an accurate GSF surface obtained from the *ab initio* calculations combined with dislocation dynamics can be used to efficiently predict the dissociation into partials, and compares well with experiments. In case of dislocation loops, however, simplifying constrained path assumptions are used to obtain the core structure. While the SVM was restricted to straight dislocations, the new model is shown to resolve the approximate nature of the core with minimum commitment to atomic details for 3D dislocations of arbitrary curvature. The force based method presented here is computationally inexpensive as well. The method can be used to study energetics of loop nucleation in perfect crystals. It is shown that the artificially introduced core-cutoff radius in current dislocation dynamics simulation can be adjusted as a function of loop size to properly account for the dislocation core energy. The advantage of the method over classical elasticity is to remove singularities from the elastic field is clearly demonstrated. The extension of the model to study dislocation transmission across interfaces in elastic bi-materials is currently underway [39]. Since the method is applicable to curved dislocations in 3D, it can be utilized to solve problems that require adequate resolution of the core structure, such as cross-slip and junction formation. In that case, it might be relevant to include the out of glide plane displacement component in the simulation.

Acknowledgements

The work conducted at UCLA was supported by the National Science Foundation through grant DMR-0113555 and by the Air Force Office of Scientific Research

(AFOSR) grant number F49620-03-1-0031. NG and NK wish to acknowledge the support from NSF-NIRT Award Number: 0506841. GL and NK acknowledge the support from the US Army grant W911NF-04-1-0058. GL also acknowledges the support from the Department of Energy grant DE-FC02-06ER25791 and from the ACS Petroleum Research Funds PRF43993-AC10.

References

[1] T. Zhu, J. Li and S. Yip, Phys. Rev. Lett. **93** 025503 (2004).
[2] S.J. Zhou, D.L. Preston, P.S. Lomdahl, *et al*., Science **279** 1525 (1998).
[3] V.V. Bulatov and E. Kaxiras, Phys. Rev. Lett. **78** 4221 (1997).
[4] G. Lu, N. Kioussis, V.V. Bulatov, *et al*., Phys. Rev. B **62** 3099 (2000).
[5] G. Schoeck, Phil. Mag. A **81** 1161 (2001).
[6] N.I. Medvedeva, O.N. Mryasov, Y.N. Gornostyrev, *et al*., Phys. Rev. B **54** 13506 (1996).
[7] J. Hartford, B. von Sydow, G. Wahnstrm, *et al*., Phys. Rev. B **58** 2487 (1998).
[8] B. Joos and M.S. Duesbery, Phys. Rev. Lett. **78** 266 (1997).
[9] J.D. Eshelby, Phil. Mag. **78** 903 (1949).
[10] J.P. Hirth and J. Lothe, *Theory of Dislocations* (Wiley, New York, 1982).
[11] J. Frenkel, Z. Phys. **37** 572 (1926).
[12] V. Vitek, Phil. Mag. **18** 773 (1968).
[13] B. Joos, Q. Ren and M.S. Duesbery, Phys. Rev. B **50** 5890 (1994).
[14] Y.M. Juan and E. Kaxiras, Phil. Mag. A **74** 1367 (1996).
[15] O.N. Mryasov, Y.N. Gornostyrev and A.J. Freeman, Phys. Rev. B **58** 11927 (1998).
[16] G. Schoeck, Phil. Mag. A **69** 1085 (1994).
[17] G. Xu, A.S. Argon and M. Ortiz, Phil. Mag. A **75** 341 (1997).
[18] J.R. Rice and G.E. Beltz, J. Mech. Phys. Solids **42** 333 (1994).
[19] L.M. Brown, Phil. Mag. **10** 441 (1964).
[20] S.D. Gavazza and D.M. Barnett, J. Mech. Phys. Solids **24** 171 (1976).
[21] W. Cai, A. Arsenlis, C.R. Weinberger, *et al*., J. Mech. Phys. Sol. **54** 561 (2006).
[22] L.P. Kubin, G. Canova, M. Condat, *et al*., Sol. Stat. Phenom. **23-24** 455 (1992).
[23] J.P. Hirth, M. Rhee and H. Zbib, J. Comp.-Aid. Mat. Desi. **3** 164 (1996).
[24] K. Schwarz, J. Appl. Phys. **85** 108 (1999).
[25] N.M. Ghoniem and L.Z. Sun, Phys. Rev. B **60** 128 (1999).
[26] N.M. Ghoniem, J. Huang and Z. Wang, Phil. Mag. Lett. **82** 55 (2001).
[27] T.C.T. Ting and D.M. Barnett, Int. J. Sol. Struct. **30**(3) 313 (1993).
[28] P.M. Anderson and Z. Li, Mater. Sci. Engng. A **319–321** 182 (2001).
[29] X. Han and N.M. Ghoniem, Phil. Mag. **83**(31–34) 3705 (2003).
[30] G. Lu, V.V. Bulatov and N. Kioussis, Phys. Rev. B **66** 144103 (2002).
[31] B.D. Wirth, V.V. Bulatov and T. Diaz de la Rubia, J. Engng Mater. Technol. **124** 329 (2002).
[32] J.P. Perdew and A. Zunger, Phys. Rev. B **23** 5048 (1981).
[33] M.J. Mills, M.S. Daw and S.M. Foiles, Ultramicroscopy **56** 79 (1994).
[34] M.S. Duesbery, in *Dislocations in Solids*, edited by F.R.N. Nabarro, Vol. 8 (North-Holland, Amsterdam, 1989), p. 67.
[35] D.J.H. Cockayne, M.L. Jenkins and I.L.F. Ray, Phil. Mag. **24** 1383 (1971).
[36] G. Xu and A.S. Argon, Phil. Mag. Lett. **80** 605 (2000).
[37] R. deWit, Sol. Stat. Phys. **10** 249 (1960).
[38] D. Rodney and R. Phillips, Phys. Rev. B **82**(8) 1704 (1999).
[39] M. Shahdeh, G. Lu, S. Banerjee, *et al*., Phil. Mag. **82**(10) 1513 (2007).